Advances in Computational Design, *Vol. 4, No. 3 (2019) 211-221*
DOI: https://doi.org/10.12989/acd.2019.4.3.211

Numerical modeling of an orthotropic RC slab band system using the Barcelona model

Paweł G. Kossakowski* and Izabela Uzarska

Department of Strength of Materials and Concrete and Bridge Structures, Kielce University of Technology, Al. Tysiąclecia Państwa Polskiego 7, 25-314 Kielce, Poland

(Received October 26, 2018, Revised January 18, 2019, Accepted January 23, 2019)

Abstract. Numerical modeling of reinforced concrete structures is a difficult engineering problem, primarily because of the material inhomogeneity. The behaviour of a concrete element with reinforcement can be analyzed using, for example, the Barcelona model, which according to the literature, is one of the most suitable models for this purpose. This article compares the experimental data obtained for an orthotropic concrete slab band system with those predicted numerically using Concrete Damage Plasticity model. Abaqus package was used to perform the calculations.

Keywords: reinforced concrete; slabs; numerical modeling; Barcelona model

1. Introduction

Modeling of concrete structures has been, and still is, a complex process. The response of this composite is certain to be inhomogeneous because the material constituents differ in their physical, chemical and mechanical properties. Analyzing non-linear behavior of a reinforced concrete element requires applying an elastic-plastic approach, like for other structural building materials (Kossakowski 2007, 2014a, 2014b). The material models used for describing the performance of geomaterials are those proposed by Drucker and Prager (D-P) (Pamin 1994, Majewski 2003) and Mohr and Coulomb (M-C) (Majewski 2003); they are models for elastic-rigid-plastic materials in which plastic flow occurs under constant stress equal to the yield stress. The Drucker and Prager model is used also for other materials (e.g. Stankiewicz and Pamin 2001), including concrete (Jiang and Wu 2012, Korol *et al*. 2017). For compression and tension regimes still other plasticity criteria are employed. The behavior of material under tension is described with the Rankine plasticiy criterion (Feenstra 1993). When concrete is in an inelastic state, stresses increase, leading to the material hardening, as well as decrease, causing its softening. The extended D-P model, known as the Barcelona model, for elastic–plastic–brittle failure, is the most suitable to describe the behavior of reinforced concrete elements (Lubliner *et al*. 1989 and Oller *et al*. 1990, Lee and Fenves 1998, Szarliński *et al*. 2002). This article describes the use of the Barcelona model to numerically analyze an orthotropic slab band system, comparing the results with the experimental data.

*Corresponding author, Ph.D., D.Sc., E-mail: kossak@tu.kielce.pl

http://www.techno-press.org/?journal=acd&subpage=7 ISSN: 2383-8477 (Print), 2466-0523 (Online)

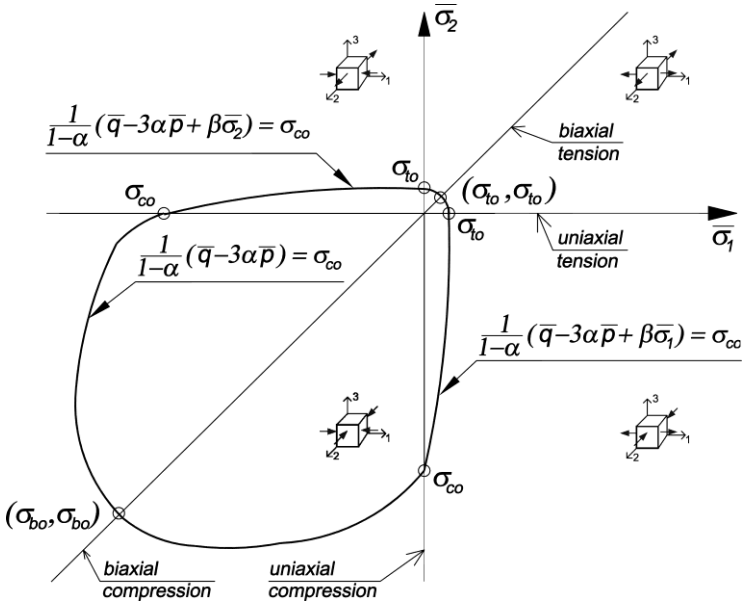

Fig. 1 Yield surface according to the 'Barcelona model' (plane stress)

2. Barcelona model

In the Barcelona model, the yield surface can be described by the following general equation:

$$f(p,q,\sigma_{ij},\chi)=F(p,q,\Theta,\chi)-\sigma_c(\chi)=0, \tag{1}$$

where: $F(p, q, \Theta, \chi)$ – a certain function of the stress invariants, p – the effective hydrostatic pressure based on first invariant J_1 ($p = -J_1/3$), q – the von Mises equivalent effective stress based on the second deviatoric stress invariant J_2 ($q = (3J_2)^{0.5}$), Θ – stress invariant, χ – the isotropic hardening variable, $\sigma_c(\chi)$ – yield stress.

The experimental data show that, in the case of (2D) plane stress, the yield surface is irregular, i.e. 'pseudo-elliptical', in shape. The Barcelona model assumes that the boundary curve is a spline curve extrapolated to the principal stress space (Abaqus Theory Manual 2002, Lubliner *et al*. 1989 and Oller *et al*. 1990).

In the Barcelona model, the general form of the yield criterion, expressed by effective stresses and based on the two-mechanism hardening law, can be written as

$$f(\overline{\sigma}_{ij},\boldsymbol{\chi})=\frac{1}{1-\alpha}\left[\overline{q}-3\alpha\,\overline{p}+\beta(\boldsymbol{\chi})\left\langle\hat{\overline{\sigma}}_{\max}\right\rangle-\gamma\left\langle-\hat{\overline{\sigma}}_{\max}\right\rangle\right]-\overline{\sigma}_c(\chi_c)=0, \tag{2}$$

where: α, β, γ – dimensionless coefficients, $\hat{\overline{\sigma}}_{max}$ – a maximum effective value of the principal stress, $\langle\cdot\rangle$ – predefined Macauley brackets:

$$\left\langle x\right\rangle=\frac{|x|+x}{2} \qquad |x|: y=\begin{cases}-x & \text{for} \quad x<0,\\ x & \text{for} \quad x\geq 0,\end{cases} \quad \boldsymbol{\chi}=\begin{bmatrix}\chi_t\\ \chi_c\end{bmatrix}. \tag{3}$$

$^{-}$ an overline denoting the effective value dependent on the degree of concrete degradation,

χ – the hardening variable for tension and compression (χ_t and χ_c, respectively).

In the biaxial compression zone, in quadrant III of the coordinate system, the equation reduces to the classical Drucker–Prager yield criterion (Oller *et al.* 1990).

$$f\left(\bar{\sigma}_{ij},\boldsymbol{\chi}\right)=\frac{1}{1-\alpha}\left[\,\bar{q}-3\alpha\,\bar{p}\right]-\bar{\sigma}\left(\chi_c\right)=0, \tag{4}$$

In quadrants II and IV, the envelopes of the elastic work zone are described by the curves using the following equations:

$$\begin{aligned} f\left(\bar{\sigma}_{ij},\boldsymbol{\chi}\right)&=\frac{1}{1-\alpha}\left(\bar{q}-3\alpha\,\bar{p}+\beta\bar{\sigma}_1\right)-\sigma_c\left(\boldsymbol{\chi}\right)=0,\\ f\left(\bar{\sigma}_{ij},\boldsymbol{\chi}\right)&=\frac{1}{1-\alpha}\left(\bar{q}-3\alpha\,\bar{p}+\beta\bar{\sigma}_2\right)-\sigma_c\left(\boldsymbol{\chi}\right)=0, \end{aligned} \tag{5}$$

In quadrant I, the yield surface is described the most often by nonlinear function, but linear relation is also observed. In latter case, for σ_1 changing from 0 to σ_{to}, the corresponding stress $\sigma_2 \approx \sigma_{to}$, and vice versa, for σ_2 changing from 0 to σ_{to}, the corresponding stress $\sigma_1 \approx \sigma_{to}$. For model shown in Figure 1, the yield surface is described by a circular sector with the stress circle radius equal to σ_{to}. In the biaxial stress condition, the parameters α, β and γ have the following form:

$$\begin{aligned} \alpha&=\frac{\sigma_{bo}-\sigma_{co}}{2\sigma_{bo}-\sigma_{co}}=const.,\\ \beta(\chi)&=\frac{\bar{\sigma}_c(\chi_c)}{\bar{\sigma}_t(\chi_t)}\left(1-\alpha\right)-\left(1+\alpha\right),\\ \gamma&=0, \end{aligned} \tag{6}$$

where: $\bar{\sigma}_c(\chi_c)$ and $\bar{\sigma}_t(\chi_t)$ – actual uniaxial compressive and tensile yield stresses, respectively, (for γ the initial phase is considered).

From the above equations, it is evident, that in the case of plane stress, the yield criterion for concrete (1) requires determining the parameters α and $\beta(0)$ on the basis of the uniaxial compressive and tensile yield stresses (σ_{co} and σ_{to}, respectively) and the biaxial compressive yield stress σ_{bo}, which are assumed to be equal in both directions.

3. Experiment

The experimental investigations were performed originally by one of the Author (Bijak [married name Uzarska] 2008) and concerned tests of slabs made of reinforced concrete.

The specimens tested were 1700 × 900 mm concrete slabs with a thickness of 60 mm. Two types of concrete slabs, differing in the mean concrete strength (f_{cm} = 39.75 MPa and f_{cm} = 22. 49 MPa), were used. The reinforcing material was 34GS steel, with the reinforcement ratios being ρ_x = 0.67% and ρ_y = 0.28%, respectively. The reinforcement system is illustrated in Fig. 2.

The slabs were tested under laboratory conditions at the Kielce University of Technology using a special facility for testing reinforced concrete elements (Bijak (Uzarska) 2008). The strain on the element was measured with point strain gages mounted in one or two rows on each side of the

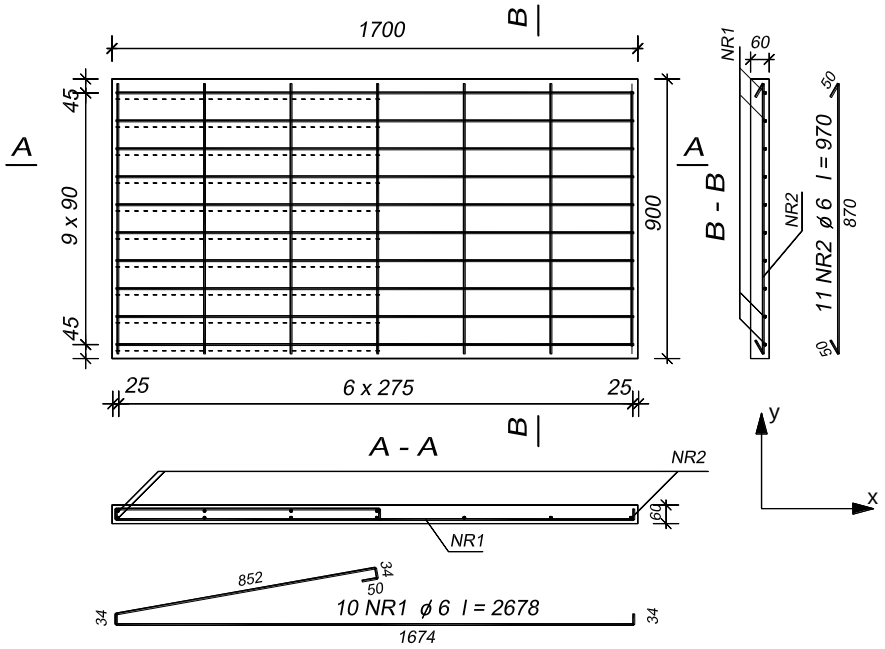

Fig. 2 Slab reinforcement system

element (six gages per row, spaced 150 mm). The slab deflection was measured using Peltron inductive displacement sensors with a measuring range of 20 mm or 50 mm fixed at 16 points, as shown in Fig. 3. The load was applied using a hydraulic jack; the load was determined by measuring the oil pressure in the universal testing machine; additionally, a strain gage load cell with a range of 0-160 kN and an accuracy of 0.12 kN was mounted on the press head (Fig. 3). The elements were loaded at the centre by applying a concentrated force. Before the tests, all the inductive displacement sensors and strain gages were calibrated and tested. Calibration required plotting a voltage-force curve for each strain gage and a voltage-displacement curve for each inductive displacement sensor. The curves were input into the program analyzing the measurement data.

The tests involved measuring the load and displacement with each increase in load F; the measurements were taken at 16 points (Fig. 3).

Additional destructive tests were carried out for cubic specimens (150×150×150 mm) to determine the compressive strength of concrete. The yield strength of steel was also determined.

4. Numerical procedure

Abaqus version 6.7, special software for finite element analysis, was applied to perform the numerical calculations (Abaqus Theory Manual 2002). The problems were solved using Abaqus Explicit. The slab geometry and the boundary conditions used in the numerical models were the same as those selected for the tests (Fig. 4).

The numerical analysis was conducted for an element under a gradually increasing load; it involved modeling the load-displacement curves obtained experimentally for the particular elements.

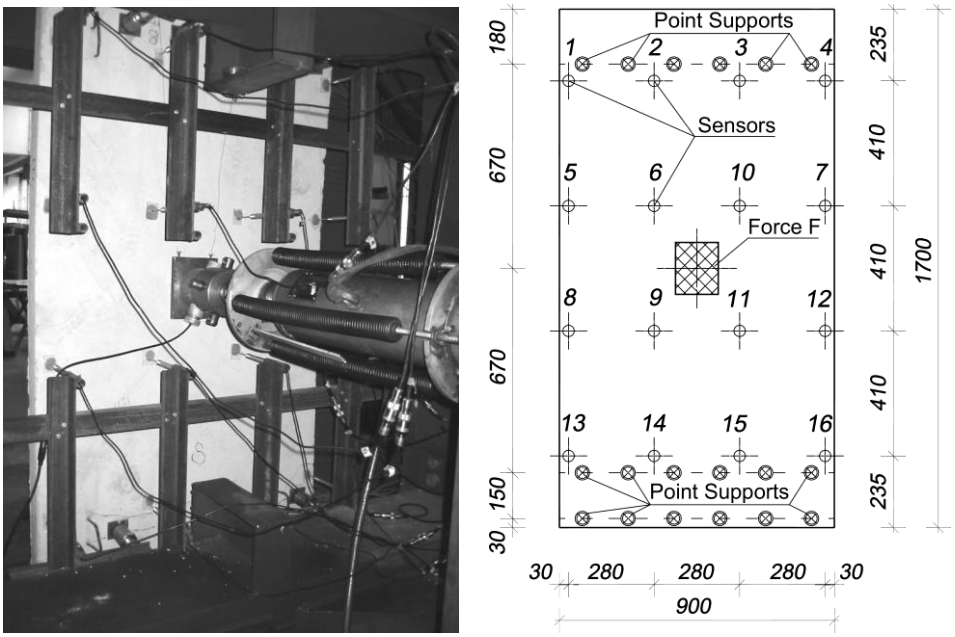

Fig. 3 Arrangement and spacing of the displacement sensors

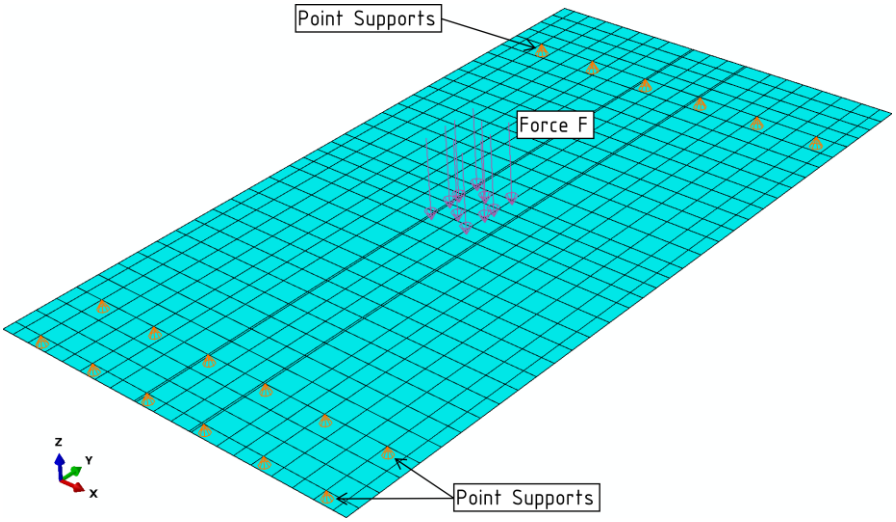

Fig. 4 Numerical model of the analyzed concrete element

The numerical models were created using standard two-dimensional four-node shell finite elements S4R (Fig. 4) from the Abaqus library. A mesh with rectangular elements was selected mainly because it was essential to precisely determine the points corresponding to the location of sensors and supports. It was easy to divide the slab into zones, with the dividing lines representing the lines along which the sensors and supports were located. The task would have been difficult if a mesh with triangular or polygonal finite elements had been used. The simulations required iteratively optimizing the finite element mesh size in order to minimize the deviation of the numerical results, i.e. load-displacement curves, from the experimental data, while keeping the

calculation time reasonable. The calculations involved applying several different models differing in the mesh density. In the generated mesh (Fig. 4), the optimum length of the sides of the finite elements ranged from about 40 to 50 mm (mean values). Such a mesh was used in the final calculations presented in this paper.

The modeling required applying a special cross-section in which the layers of the slab reinforcement (reinforcing mesh) were the same as those in the element tested.

A built-in function was used to define the reinforcement in the cross-section of the *shell*-type element. The Abaqus procedure involved defining the layers of uniaxial reinforcement and adding the rebars to the cross-section, which, for shell elements, are treated as smeared layers with a constant thickness equal to the area of each reinforcing bar divided by the reinforcing bar spacing. The reinforcement was in the form of ø6 bars arranged orthogonally in two, i.e. upper and lower, layers. The numerical calculations provided a faithful representation of the reinforcement of the physically tested elements (Fig. 2). The cross-sectional area of the rebar was defined with respect to a local coordinate system. The rebar geometry was constant, defined by area per bar; for the ø6 bar, A = 28.2735 mm^2, and the bar spacing, s, was 90 and 275 mm, for the longitudinal and transversal directions, respectively. For the orthotropic slab system, the orientation angles were 0° and 90°. Since shell-type finite elements were used, the position of the rebar layers in the shell thickness was defined according to the real geometry (Fig. 2).

The basic material parameters assumed for the concrete and the reinforcement steel were the same as those for isotropic materials, taking into account the quantities determined during the destructive tests. The model with perfect plasticity for the reinforcement steel was applied.

The slab support was assumed to be in the form of point support, as shown in Fig. 4, to prevent displacements along the direction perpendicular to the slab surface (the z direction). The load imposed on the slab (force F) was distributed across the surface in contact with the actuator plunger, like during the experiment (Fig. 3).

The concrete behavior was predicted by means of a special model of plastic material known as the *Concrete Damage Plasticity* model, currently very popular and still modified (Lee and Fenves 1998, Jankowiak and Łodygowski 2005, Kmiecik and Kamiński 2011, Belletti *et al*. 2015, Wosatko *et al*. 2015, Genikomsou and Polak 2015 and 2017, Alfarah *et al*. 2017, Szczecina and Winnicki 2017, Wosatko *et al*. 2018, Goh and Hrynyk 2018).

The plastic range for concrete was defined with the following parameters: Ψ = 15º, ε = 0.1, σ_{b0}/σ_{c0} = 1.16, K_c = 2/3 and m = 0 (Cińcio and Wawrzynek 2003). The compression range was determined on the basis of the stress-strain curve (Majewski 2003) using the following relationship:

$$\sigma(\varepsilon) = f_c \frac{x(k-x)}{1-(2-k)x}, \qquad x = \frac{\varepsilon}{\varepsilon_c}, k = \frac{E_o \varepsilon_c}{f_c} \tag{7}$$

where: e_c= – 0.0022

The tensile strength of concrete was calculated from the ratio of the uniaxial tensile stress to the uniaxial compressive stress: $m_t = f_t/f_c$. In his review article, Oluokun (1991) indicates that $m_t = 0.3296\, f_c^{-0.3376}$.

In the case of tension (Szarliński 2002), the material softening function for the σ–ε curve was derived from:

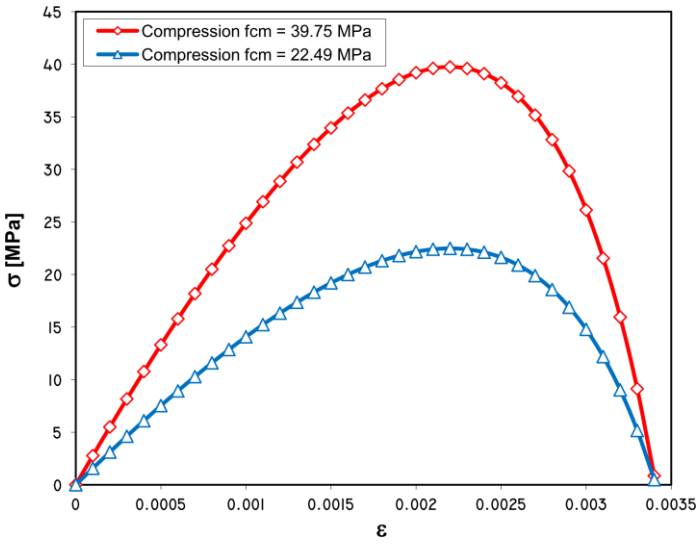

Fig. 5 σ-ε relationship used in the numerical analysis of the concrete in the compression zone

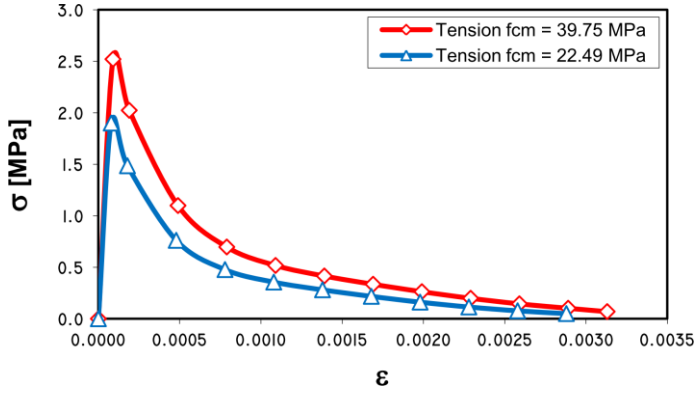

Fig. 6 σ-ε relationship used in the numerical analysis of the concrete in the tension zone

$$\sigma(\varepsilon) = f_t \left\{ \left[1 + \left(c_1 \frac{\varepsilon}{\varepsilon_u} \right)^3 \right] \exp\left(-c_2 \frac{\varepsilon}{\varepsilon_u} \right) - \frac{\varepsilon}{\varepsilon_u} \left(1 + c_1^3 \right) \exp\left(-c_2 \right) \right\} \tag{8}$$

assuming that

$$c_1 = 3.0, \quad c_2 = 6.93,$$

$$\varepsilon_u = \frac{5.14 G_f}{w f_t}, \qquad w = 2\pi l,$$

where: G_f is the fracture energy determined in accordance with the CEB-FIP Model Code of 1990 (1993)

$$G_f = \alpha_F f_c^{0.7} \tag{9}$$

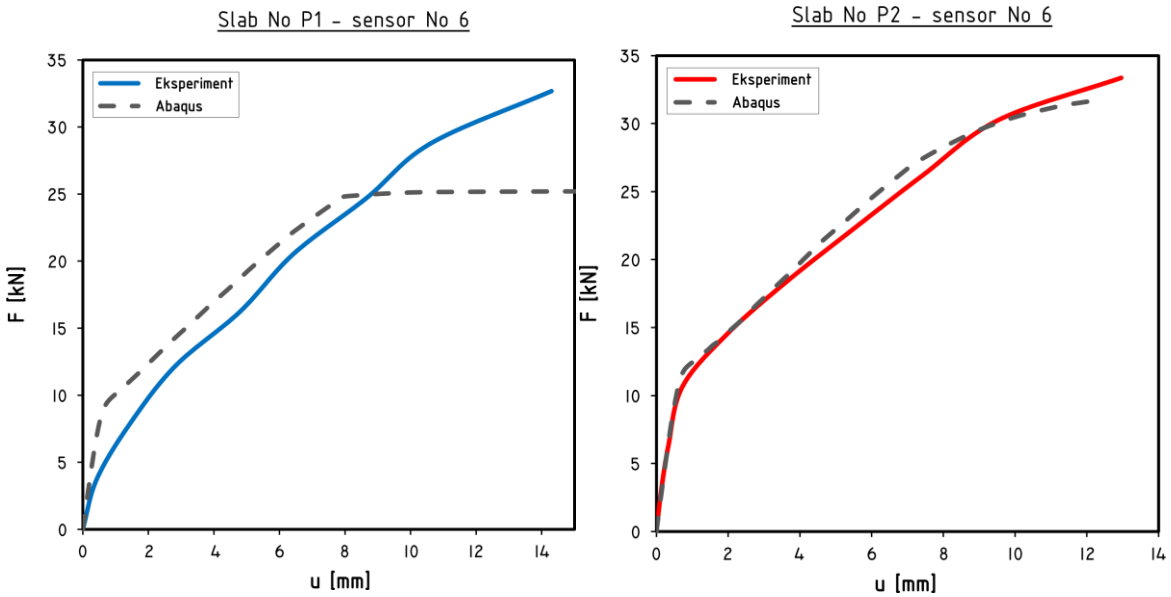

(a) slab P1 at f_{cm} = 22.49 MPa (b) slab P2 at f_{cm} = 39.75 MPa

Fig. 7 Force (F) against displacement (u) obtained numerically and experimentally with sensor No. 6

where: $\alpha_F = 6$ – coefficient dependent on the maximum aggregate grain size [3], f_c – cylindrical compressive strength of concrete $f_{15/30}$, assuming that $f_c = f_{cm}/1.25$.

The reinforcement steel was analyzed by employing a model of elastic-plastic material response, defined with the following quantities: E = 205 GPa, ν = 0.3 and R_e = 476.2 MPa.

5. Results

Figure 7 shows the force–displacement plots obtained numerically using the *Concrete Damage Plasticity* model which are compared with the experimental data recorded by sensor No. 6 for slabs (f_{cm} = 22.49 MPa and f_{cm} = 39.75 MPa) over a full range of loads.

As can be seen, there is good agreement between the numerical and experimental results obtained for the slabs at f_{cm} = 39.75 MPa (Fig 7b), while there is no such agreement for the slabs with lower mean concrete strength (Fig. 7a). In the latter case, the numerically calculated values of the force F for the displacement u ranging from 0 mm to about 8 mm were slightly higher than those determined experimentally. It should be noted, however, that the numerical and experimental curves generated for this displacement range are similar. When u = 8 mm, the numerically simulated force F remained stable whereas the experimentally determined force continued to rise. It was thus it was difficult to analyze and compare the strain distributions obtained experimentally and numerically. The representative contour plots for a concrete slab of higher strength denoted as P2 are shown and analyzed below.

Figure 8 provides mapping results for strains ε_{11} and ε_{22} for a concrete slab at f_{cm} = 39.75 MPa.

Figure 9 shows the main plastic strains and the crack pattern determined experimentally for a slab with a mean concrete strength of 39.75 MPa.

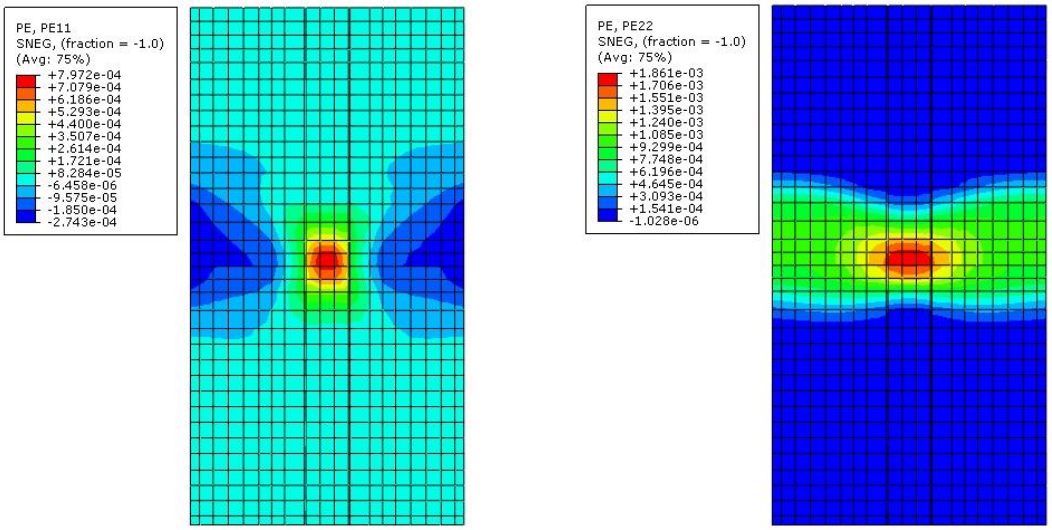

(a) strain ε_{11} (b) strain ε_{22}

Fig. 8 Strain mapping for ε_{11} and ε_{22} for slab P2 at F = 15.69kN

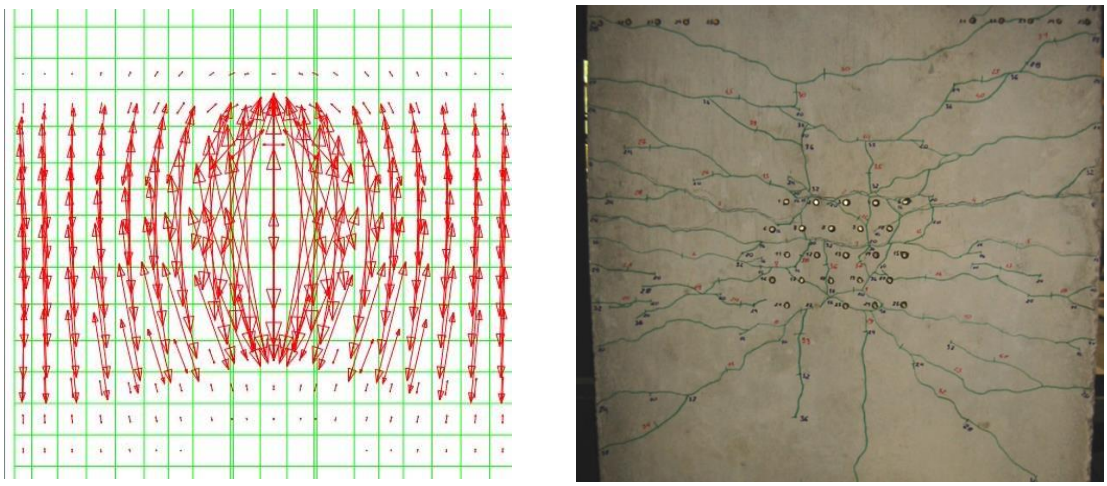

(a) main plastic strains (b) crack pattern

Fig. 9 Damage results for slab P2

The simulated distributions of the plastic strains ε_{11} and ε_{22} for slab P2 at F = 15.69 kN show that the strain concentrations are higher on the bottom surface and in the central part of the slab (Figs. 8a and b). The extreme values of the calculated plastic strains in this area are of a similar order of magnitude, and they are: $\varepsilon_{11} = 7.972\times10^{-4}$ and $\varepsilon_{22} = 1.861\times10^{-3}$. The ratio of these values is the same as the ratio $\varepsilon_{11}/\varepsilon_{22}$ predicted for the slab with the analyzed ratio of sides. These results including the simulated principal strain directions (Fig. 9a) well correspond with the actual cracks on the bottom surface of the slab (Fig. 9b). The numerically determined principal strain directions and the strain concentrations well correspond to the crack morphology observed after the destructive tests.

6. Conclusions

This article has discussed results of a numerical analysis performed with a failure model for plastic-brittle material and compared them with the experimental data obtained for an orthotropic slab band system made of two types of concrete differing in the mean concrete strength. The findings were used to draw the following conclusions for analyzed elements:

- the differences between the numerical and experimental data observed for the slab at f_{cm} = 22.49 MPa indicate that the load-carrying capacity predicted numerically is about 30% lower than that reported during the experiments, and the displacement, which ranges from 50% to 10%, is smaller than that obtained through tests,
- there is good agreement between numerical and experimental results concerning displacement and load-carrying capacity for slabs at f_{cm} = 39.75 MPa.

From the results obtained for the analyzed elements, it is clear that the Barcelona model was suitable to model slab elements made of standard grade concrete. For lower grade concrete, however, modification of the model parameters may be necessary. It seems that, in such a case, the steel hardening effect should be taken into consideration and defined for the material properties of reinforcement in numerical simulations. This will allow us to increase the total load-carrying capacity of elements when steel reinforcement is yielding.

Obviously, more complex analysis for elements differing in geometry and concrete grade is required to further explain the observed phenomena and modify the model parameters.

References

Abaqus Theory Manual (2002), ABAQUS v.6.3.1, Hillerborg, Hibbit, Karlsson and Sorensen, Inc.

Alfarah, B., López-Almansa, F. and Oller, S. (2017), "New methodology for calculating damage variables evolution in plastic damage model for RC structures", *Eng. Struct.,* **132**, 70-86. https://doi.org/10.1016/j.engstruct.2016.11.022.

Belletti, B., Walraven, J.C. and Trapani, F. (2015), "Evaluation of compressive membrane action effects on punching shear resistance of reinforced concrete slabs", *Eng. Struct.*, **95**, 25-39. https://doi.org/10.1016/j.engstruct.2015.03.043.

Bijak (Uzarska), I. (2008), "Degradacja sztywności płyt żelbetowych w procesie krótkotrwałych obciążeń niskocyklicznych", Ph.D. Dissertation, Kielce University of Technology, Kielce, Poland.

CEB-FIP Model Code 1990 (1993), *CEB-FIP Model Code 1990,* Bulletin d'information, no. 1996; International Federation for Structural Concrete; Lausanne, Switzerland.

Cińcio, A. and Wawrzynek, A. (2003), "Plastyczno-kruchy degradacyjny model betonu w symulacjach numerycznych konstrukcji obciążonych cyklicznie", *Sci. Papers Silesian U. Technol.*, 1-11.

Feenstra, P.H. (1993), "Computational aspects of biaxial stress in plain and reinforced concrete", Ph.D. Dissertation, Delft University of Technology, Delft, The Netherlands.

Genikomsou, A.S. and Polak, M.A. (2015), "Finite element analysis of punching shear of concrete slabs using damaged plasticity model in ABAQUS", *Eng. Struct.*, **98**, 38-48. https://doi.org/10.1016/j.engstruct.2015.04.016.

Genikomsou, A.S. and Polak, M.A. (2017), "Finite element simulation of concrete slabs with various placement and amount of shear bolts", *Procedia Eng.*, **193**, 313-320. https://doi.org/10.1016/j.proeng.2017.06.219.

Godlewski, G. Ł. (2007), "Analiza wpływu D_{max} na parametry mechaniki pękania betonów wapiennych określane przy trójpunktowym zginaniu", *Budownictwo i Architektura*, **1**, 5-16.

Goh, C.Y.M. and Hrynyk, T.D. (2018), "Numerical investigation of the punching resistance of reinforced

concrete flat plates", *J. Struct. Eng.*, **144**(10), https://doi.org/10.1061/(ASCE)ST.1943-541X.0002142.
Jankowiak, T. and Łodygowski, T. (2005), "Identification of parameters of concrete damage plasticity constitutive model", *Foundations of Civil and Environmental Engineering*, **6**, 53-69.
Jiang, J.F. and Wu, Y.F. (2012), "Identification of material parameters for Drucker-Prager plasticity model for FRP confined circular concrete columns", *J. Solids Struct.*, **49**(3-4), 445-456. https://doi.org/10.1016/j.ijsolstr.2011.10.002.
Kmiecik, P. and Kamiński, M. (2011), "Modelling of reinforced concrete structures and composite structures with concrete strength degradation taken into consideration", *Arch. Civil Mech. Eng.*, **11**(3), 623-636. https://doi.org/10.1016/S1644-9665(12)60105-8.
Korol, E., Tejchman, J. and Mróz, Z. (2017), "Experimental and numerical assessment of size effect in geometrically similar slender concrete beams with basalt reinforcement", *Eng. Struct.*, **141**, 272-291. https://doi.org/10.1016/j.engstruct.2017.03.011.
Kossakowski, P.G. (2014a), "Stress Modified Critical Strain criterion for S235JR steel at low initial stress triaxiality", *J. Theoretical Appl. Mech.*, **52**(4), 995-1006. https://doi.org/10.15632/jtam-pl.52.4.995.
Kossakowski, P.G. (2014b), "An analysis of the Tvergaard parameters at low initial stress triaxiality for S235JR steel", *Polish Maritime Res.*, **21**(4), 100-107. https://doi.org/10.2478/pomr-2014-0046.
Kossakowski P.G. (2007), "Influence of anisotropy on the energy release rate G_I for highly orthotropic materials", *J. Theoretical Appl. Mech.*, **45**(4), 739-752.
Lee, J. and Fenves, G.L. (1998), "Plastic-damage model for cyclic loading of concrete structures", *J. Eng. Mech.*, **124**(8), 892-900. https://doi.org/10.1061/(ASCE)0733-9399(1998)124:8(892).
Lubliner, J., Oliver, J., Oller, S. and Oñate, E. (1989), "A plastic-damage model for concrete", *J. Solid Struct.*, **25**(3), 299-326. https://doi.org/10.1016/0020-7683(89)90050-4.
Oller, S., Oñate, E., Oliver, J. and Lubliner, J. (1990), "Finite element nonlinear analysis of concrete Structure using a plastic-damage model", *Eng. Fracture Mechanics*, **35**(1/2/3), 219-231. https://doi.org/10.1016/0013-7944(90)90200-Z.
Majewski, S. (2003), *Mechanika betonu konstrukcyjnego w ujęciu sprężysto –plastycznym*, Wydawnictwo Politechniki Śląskiej, Gliwice, Poland.
Oluokun, F.A. (1991), "Prediction of concrete tensile strength from compressive strength: An evaluation of existing relations for normal weight concrete", *ACI Mater. J.*, **88**(3), 302-309.
Pamin, J.K. (1994), "Gradient-Dependent Plasticity In numerical simulation of localization phenomena", Ph.D. Dissertation, Delf University of Technology, Delft, the Netherlands.
Stankiewicz, A. and Pamin, J. (2001), "Simulation of instabilities in non-softening Drucker-Prager plasticity", *Comput. Assisted Mech. Eng. Sci.*, **8**(1),183-204.
Szarliński, J., Winnicki, A. and Podleś, K. (2002), *Konstrukcje z betonu w płaskich stanach*, Cracow University of Technology, Cracow, Poland.
Szczecina, M. and Winnicki, A. (2017), "Relaxation time in CDP model used for analyses of RC structures", *Procedia Eng.*, **193**, 369-376. https://doi.org/10.1016/j.proeng.2017.06.226.
Wosatko, A., Pamin J. and Polak, M.A. (2015), "Application of damage–plasticity models in finite element analysis of punching shear", *Comput. Struct.*, **151**, 73-85. https://doi.org/10.1016/j.compstruc.2015.01.008.
Wosatko, A., Genikomsou, A., Pamin, J., Polak, M.A. and Winnicki, A. (2018), "Examination of two regularized damage-plasticity models for concrete with regard to crack closing", *Eng. Fracture Mech.*, **194**, 190-211. https://doi.org/10.1016/j.engfracmech.2018.03.002.